E14-2008-77

A. S. Khalil [1,*], A. Yu. Didyk [**]

DISORDERED ZONES BY 100 keV Au^+ ION IRRADIATION IN INDIUM PHOSPHIDE: DIRECT OBSERVATIONS AND *IN-SITU* TEM ELECTRON-BEAM-INDUCED RECOVERY

Submitted to «Particles and Nuclei, Letters»

[1] Tabbin Institute for Metallurgical Studies, Cairo, Egypt
[*] E-mail: skhalil2004@yahoo.com
[**] E-mail: didyk@jinr.ru

Халиль А. С., Дидык А. Ю. E14-2008-77

Области разупорядочения в фосфиде индия. Изучение *in-situ* стадии возврата структуры при воздействии ПЭМ-электронов

Методом просвечивающей электронной микроскопии (ПЭМ) исследованы изолированные деструктированные области в InP, образованные в результате облучения ионами золота с энергией 100 кэВ при комнатной температуре и являющиеся «зародышами» для достижения полной аморфизации при достижении флюенсов $\sim 2{,}5 \cdot 10^{13}$ ион/см^2. Накопление дефектов при облучении ионами Au с энергией 100 кэВ описано с использованием композитной теоретической модели при учете гомогенного и гетерогенного процессов аморфизации.

Стадия возврата разупорядочения в форме изолированных областей была инициирована последующим облучением электронами *in-situ* при ПЭМ-исследованиях. Суммарная доля деструктированных областей уменьшается как сложная функция, зависящая от флюенса электронов во всем интервале изученных энергий (100–300 кэВ). ПЭМ-исследования *in-situ* деструктированных областей показывают, что стадия возврата этих областей зависит от облучения электронами, от их энерговыделения, но вклады от прямого упругого смещения атомов In и P недостаточны для такого возврата. Таким образом, можно сделать вывод, что неупругие потери электронов играют доминирующую роль при отжиге неупорядоченных областей.

Работа выполнена в Лаборатории ядерных реакций им. Г. Н. Флерова ОИЯИ.

Препринт Объединенного института ядерных исследований. Дубна, 2008

Khalil A. S., Didyk A. Yu. E14-2008-77

Disordered Zones by 100 keV Au^+ Ion Irradiation in Indium Phosphide:
Direct Observations and *In-situ* TEM Electron-Beam-Induced Recovery

Transmission Electron Microscopy (TEM) has been used to observe the spatially isolated disordered zones in InP resulting from 100 keV Au ion irradiation at room temperature which act as precursor structure for reaching complete amorphization of the top layer at ion fluences $\sim 2.5 \cdot 10^{13}$ ions/cm^2. The accumulation of damage due to the 100 keV Au ion irradiation was described in this material using a composite theoretical model accounting for both homogeneous and heterogeneous amorphization processes.

Recovery of disorder in the form of spatially isolated disordered zones was induced by electron irradiation and was characterized by *in-situ* TEM observation. The total areal fraction of the disordered zones in initial electron pre-irradiated InP decreased as a function of irradiating electron fluence within all the investigated electron energy range (100–300 keV). The *in-situ* TEM recovery of disordered zones shows that these zones are sensitive to electron beam irradiation and recover even under electron energies not sufficient to directly elastically displace lattice atoms, i.e., subthreshold energies for both constituent atoms In and P. This implies that inelastic electron energy loss processes might play a dominant role for disordered zone recovery.

The investigation has been performed at the Flerov Laboratory of Nuclear Reactions, JINR.

Preprint of the Joint Institute for Nuclear Research. Dubna, 2008

INTRODUCTION

The formation of spatially isolated disordered and/or amorphous zones by low-energy heavy-ion irradiation in semiconductor materials and their subsequent electron irradiation-induced recovery (annealing) have recently received much attention [1]. Both fundamental and technological insights are gained by investigating the evolution of these zones as they represent the precursor structures from which a continuous amorphous layer is formed in implanted semiconductor devices when the irradiating ion fluences reach levels to cause complete amorphization of top layer. Molecular dynamics simulations and other theoretical investigations of the damage caused by energetic heavy ion implanted in semiconductor substrates have revealed that a characteristic feature is the presence of disordered/amorphous zones created by the release of large amount of kinetic energy in local regions [2]. These zones can account for part or most of the produced damage in the irradiated material, the extent of which depends on the crystal structures and bond strengths of target material. Thus, as the ion fluences increase, these zones overlap until a continuous amorphous layer is formed. It has been demonstrated that electron irradiation at an energy lower than the threshold energy required to produce direct atomic displacement has resulted in zone shrinkage and disappearance in several elemental and compound semiconductors [3]. The disappearance rate of thermally and laser-induced recovery of these zones was compared to the electron beam-induced recovery process and it was found that the electron beam-induced recovery was more efficient (judged by the disappearance rate vs elapsed time) than the first two processes [4].

Since the first direct TEM observation of disordered zones in an irradiated elemental semiconductor by Parsons et al. [5], many TEM investigations have been performed. An extensive TEM investigation of isolated disordered zones in Si and Ge has been described by Howe et al. [6]. In their investigations, irradiations were performed at low temperatures $T < 50$ K using a range of heavy ions from P^+ to Bi^+ ions into Si and from As^+ to Bi^+ ions into Ge at energies between 10 and 120 keV. For heavier ions, the diffraction contrast of zones observed in TEM was stronger than that for lighter ions, which may be explained by the denser cascades in the case of heavier ions. From diffraction contrast experiments it was concluded that the damage could be *best* described as amorphous

in nature. In another study, high resolution transmission electron microscopy (HRTEM) observation of heavy-ion irradiated Si at 4 K by Narayan et al. [7] revealed that the damaged zones were *indeed* amorphous in nature. In contrast, Howe and Rainville [8] suggested that the damage level in the peripheral regions of the zones had simply become large enough to produce diffraction contrast observed by TEM. HRTEM by Ruault et al. [9] was used to investigate individual zones in 50–200 keV Bi^+ ion irradiated Si. They noted that the core was amorphous in nature. The TEM observation revealed that core diameters were not sufficiently large to explain the formation of an amorphous layer at fluences $\sim 6 \cdot 10^{12}$ ions/cm^2. *In-situ* observations showed that when the ion fluence was increased and strongly contrasting damaged regions began to overlap, additional regions appeared with characteristic weaker contrast than that exhibited by the damaged cores produced in completely isolated zones. It was suggested that the overlap of these weaker contrast damaged regions outside the amorphous cores was responsible for the progression of amorphization. These regions, termed *gray* zones, first began to appear in the area between existing strong contrasts regions [10]. At higher fluences both the strong dark contrast defects and the «gray zones» increasingly overlapped. The authors conclude that gray zones represent a separate amorphous state distinct from the amorphous zones themselves inside the cores and that these play some role in the total amorphization process, although no satisfactory explanation is given to support this idea. However, in an earlier observation by Chadderton [11] in 100–400 keV Bi^+ irradiated Si, it was found that for irradiation at room temperature, *some* but not all of the observed disordered zones could be described as amorphous. In the case of compound semiconductors irradiated by heavy ions, we cite the earlier work of Chandler and Jenkins [12] and especially the work of Jenkins [13] on 100 keV irradiation of different heavy-ion species in the compound semiconductors GaAs and GaP. *Spot* damage was observed in GaP which exhibited the same structure factor contrast as Si and Ge. The defect yield, defined as the ratio of the ion fluence to the observed zone density, was close to unity for all ion damage in GaP, and the average diameter of the damaged regions was $\sim$ several nm. These observations led to the conclusion that zones in GaP were amorphous. In comparison, the damage in GaAs consisted of a very low density of weak TEM contrast features that could not be identified unambiguously. In the case of InP, spatially isolated zones in InP irradiated with 50 keV Si^+ ions at room temperature were investigated using TEM [14]. A diffuse ring characterizing the onset of amorphization appeared in the electron diffraction pattern at irradiation fluences $\sim 2 \cdot 10^{13}$ ions/cm^2. Complete amorphization was ascribed to the previously mentioned overlap of the gray zones as for the case of the irradiated elemental semiconductor Si advocated by the same investigators [9, 15]. An important observation was that these zones were found to shrink and disappear during prolonged TEM observation at electron beam energies $\geqslant 100$ keV at room temperature [14]. More recent TEM observations

of isolated zones following ion irradiation have been reported in the compound semiconductors GaAs, GaP, InP (in addition to the elemental semiconductors Si and Ge) [1, 3, 4, 16–21]. However, the authors assumed that the observed zones in *all* the compound and elemental semiconductors investigated were amorphous in nature, based on TEM observations of zones for *only* GaAs irradiated with heavy ions [3] which appear as dark contrast irregular features in conventional TEM. These zones exhibit amorphous cores as revealed by HRTEM. In this series of investigations by Jencic et al. [16–21], TEM image computer analysis was used to extract the recovery behaviour during *in-situ* electron irradiation. Zone diameters — based on approximating the area of irregular zone morphology to a circle — were reported to shrink linearly with increasing electron fluence, the shrinkage rate falling with decreasing electron energy. The observed shrinkage rate fell to a minimum at electron beam energies corresponding to elastic energy transfers $\sim 0.5E_d$, (where E_d is the displacement energy which was assumed to be an *overall average* atomic displacement energy neglecting crystalline directional dependencies). Surprisingly, the shrinkage rate increased again at lower electron energies ($\leqslant 100$ keV) and was found to be insensitive to the crystallographic orientation and the temperature at which the *in-situ* electron irradiation was carried out. These experiments clearly suggest that low-energy electron beam recovery does not require point defects production by direct elastic atomic displacement but rather than electron excitation and ionization effects (inelastic) may be responsible for the surprising observations. Recent MD simulations [22] have shown that the process of recovery for amorphous zones in subthreshold electron irradiation of Si might be not only due to the elastic energy transfer but also by inelastic processes involving, for example, bond breakage and a rearrangement of the disrupted atomic order at the amorphous-zone/crystal lattice interface.

In the present investigation, we further investigate the formation, accumulation and electron beam-induced recovery of disordered zones produced by low-energy Au ion irradiation in InP followed by direct TEM observation, RBS/C and by *in-situ* TEM electron irradiation.

1. EXPERIMENTAL STUDIES

InP samples were prepared for irradiation from a 500 μm thick, semi-insulating, polished, (001) oriented InP wafer; each bulk sample being scribed and cut into pieces of $\sim 10 \times 10$ mm for ion irradiation. In addition to bulk samples, thin foil samples (electron transparent $\leqslant 200$ nm thick) were prepared before the ion irradiation in order to avoid the artifacts usually associated with post-irradiation preparation of InP and to facilitate the immediate TEM observation of the irradiated samples. The thin foils were prepared by first coring 3 mm disks

from slivers of the (001) InP wafer. The disks were then mechanically ground and dimpled to a thickness of 100 μm before being chemically thinned to perforation in 2% bromine-methanol solution. Both the bulk and thin foil samples were irradiated by 100 keV Au ions in a non-channelling direction at room temperature using the tandem accelerator at the Electronic Materials Engineering department at the ANU. The ion fluence ranged from $1 \cdot 10^{12} - 1 \cdot 10^{14}$ ions/cm^2 and the ion flux was $\sim 5.7 \cdot 10^{11}$ ions/cm^2/s. Subsequently the irradiated bulk samples were analyzed by Rutherford Backscattering with 2 MeV He^+ ions, and a glancing scattering angle of $\sim 120^\circ$. The TEM and *in-situ* electron irradiation were performed in Phillips CM-300 microscope. The electron irradiations were carried out using the illuminating electron beam as functions of both electron beam energy and fluence. The electron dosimetries were quantified for electron beam energies ranging from 100 to 300 keV. The beam current was first accurately measured at 300 keV ($i_{\max} = 8.3 \pm 1.6$ nA) using a Gatan analytical double tilt holder fitted with an electrically isolated Faraday cup. The beam was then spread to cover the circular viewing fluorescent screen at magnifications sufficient to observe and analyze the disordered zones ($\sim$ 70 KX) and the exposure time which determines the beam intensity falling on the fluorescent screen (at this current) was acquired (as indicated by the exposure meter in the TEM panel). Beam profiles falling on the sample for the other used energies were obtained to ensure the uniformity of electron flux over the beam widths. The beam diameter at full width half maximum (FWHM) was determined for each beam energy (100–300 keV) and was ~ 2 μm. By scaling the exposure times for each energy to that acquired for 300 keV for which an accurate electron beam current has been measured, estimations for beam currents were obtained. Thus, during electron irradiations, the electron beam was spread over a radius ~ 2 μm where the beam has a uniform profile. For each experiment the flux was maintained constant and hence the total electron fluence was proportional to the irradiation time. The current density irradiating the samples (J) was in the range $0.1 \leqslant J \leqslant 0.4$ A $\cdot$ cm^{-2}. The contrast of the obsereved zones was enhanced by using bright field technique down the $\langle 001 \rangle$ zone axis, where these zones generally appear as irregular dark contrast features in a homogeneous light background. And the *in-situ* electron irradiation was conducted axially along the $\langle 001 \rangle$ zone axis to investigate electron-beam-induced recovery of disorder created by 100 keV Au^+ ion irradiation of InP. Thus, a field of many disordered zones was identified in an area of the lowest ion fluence irradiated InP sample ($1 \cdot 10^{12}$ ions/cm^2) and the evolution of that initial disorder under electron beam irradiation in TEM was *in-situ* monitored. The evolution of disorder under electron beam irradiation was investigated for five different electron beam energies ranging from 100 to 300 keV. Thus, each *in-situ* TEM observation for particular electron beam energy rendered a series or time sequence of TEM images which enabled us to access the TEM observed recovery of the initial disorder with the irradiating electron fluence for the corresponding

electron energy. The images were digitized, computer processed using Adobe Photoshop software to enhance the overall images quality and improve contrast, subsequently the analySiS software package [23] was used for quantitative image analyses (to estimate the total area of the observed disorder for each image in a sequence). It is relative straightforward to measure an irregularly shaped feature such as single zone from a digitized image. However, for an image with a field of many irregularly shaped features (disordered zones) of different contrast levels (different gray levels) as obtained in a typical TEM image, difficulties may arise in setting threshold levels for that digitized image for the subsequent computer analysis as the effect of altering the threshold even slightly can be quantitatively large [24]. To find the optimum threshold levels, visually judged by observing the best levels that define and encompass almost all the observed different dark contrast features (zones) for all the images in a particular TEM image sequence, hence, a set of S-shaped graphs for micrographs of each sequence was obtained based upon continuous threshold level variation (the abscissa) and the corresponding calculated total areal fraction of all the dark contrast (the ordinate) vs threshold level values. We found that the optimum threshold levels lie (on the abscissa) at approximately $\sim 50\%$ of the value of the threshold level of the inflection point on the second derivative graphs of these S-shaped graphs. It was found that this delivered the best and maximum definition of all the disordered zone boundaries in the same sequence of TEM images. Hence, this image optimization process was carried out for each series of the obtained TEM images (i.e., for every TEM image sequence of the investigated electron beam energies).

2. RESULTS AND DISCUSSION

Isolated disordered zones visible in TEM display a characteristic contrast. These zones appear in TEM as dark irregular features of different sizes distributed over the irradiated area. Figure 1 shows this characteristic Spot contrast in 100 keV Au^+ ion irradiated InP. The micrograph was obtained under BF conditions along the $\langle 001 \rangle$ zone axis, chosen so as to improve both resolution and contrast [25, 26]. An image of an unirradiated sample is shown for comparison, displaying only the observed simple extinction contours, where regions of the crystal satisfy the Bragg condition for the imaging electrons.

The contrast is similar to that observed in other irradiated compound semiconductor materials [1], where the irregular strain contrast observed by TEM maps the boundary of a three-dimensional disordered zone. The contrast arises predominantly from strain in the lattice surrounding the damaged «core» resulting from a cascade which might, for example, contain a distribution of point defects or point defect clusters and/or amorphous material. This lattice disorder and associated strain-fields scatter (diffract) illuminating electrons which give rise

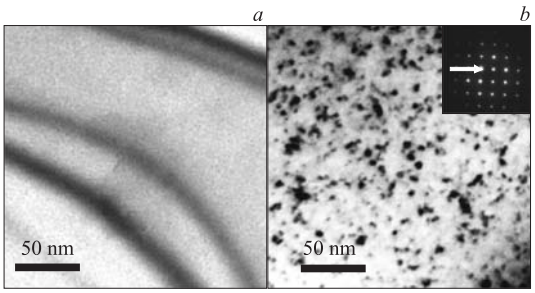

Fig. 1. BF-TEM of (a) sample before irradiation and (b) residual disorder following 100 keV Au^+ ($1{\cdot}10^{12}$ ions/cm^2) irradiation in InP imaged along [001] zone axis orientation (in the SADP inset the arrow points to the transmitted «undiffracted» beam)

to the dark features observed in BF-TEM. Diffraction patterns (inset in Fig. 1, b) observed at these relatively low-ion fluences ($1 \cdot 10^{12}$ ions/cm^2) exhibit the sharp spots associated with unirradiated InP, there were no rings, diffuse or otherwise. Given that the total volume of the defective material is relatively small compared to the intact surrounding matrix, it is possible that they might indeed be amorphous and the rings are simply too diffuse to be detectable. The possibility that the disordered zones might be simply an agglomeration of point defects and not amorphous in nature or a combination of both must be considered. In Fig. 2 a sequence of RBS/C spectra is presented for InP samples irradiated by 100 keV Au^+ ions up to a fluence of $1 \cdot 10^{14}$ ions/cm^2. It should be noted that there exists a minimum between the surface peak and the damage peak which persists, even for fluences between $5 \cdot 10^{12}$ and $1 \cdot 10^{13}$ ions/cm^2. This implies that damage is relatively low and that some crystallinity remains for this depth. For the sample irradiated to $1{\cdot}10^{12}$ ions/cm^2, the RBS/C spectrum shows that the amount of dam-

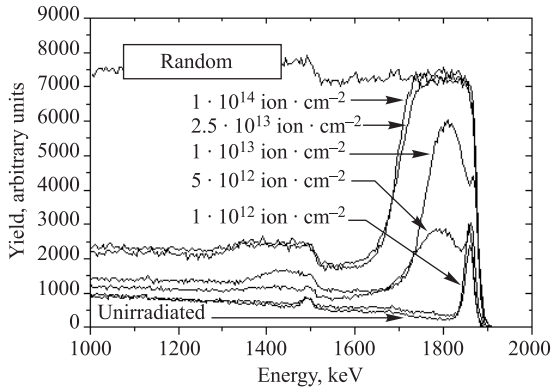

Fig. 2. RBS/C spectra of 100 keV Au^+ irradiated InP for different ion fluences

age is noticeably low compared to higher fluences and is barely distinguishable from the unirradiated sample. However, the damage at this relatively low fluence is clearly evident as disordered zones which are revealed by TEM (Fig. 1). This indicates the higher relative sensitivity and the merit of TEM analysis at lower irradiation fluence regimes when compared to RBS/C analysis.

The RBS/C yield increases with increasing fluence are consistent with an increase in disorder build-up in InP. When the irradiated InP becomes completely amorphous, the yield generally arrives at the random level. Thus, at fluences $\sim 2.5 \cdot 10^{13}$ ions/cm^2 the backscattered spectrum has reached the random level indicating that the surface layer is amorphized. The thickness of the amorphous layer was calculated to be 45 ± 5 nm. This is in a reasonable agreement with the value of $R_p + \Delta R_P = 36.4$ nm (where $R_p = 26.3$ nm is the 100 keV Au$^+$ ion range in InP and $\Delta R_P = 10.1$ nm is the longitudinal straggling calculated from SRIM [27] simulations of 100 keV Au ions into InP). The mechanism of damage accumulation can be better understood by analysing the fluence dependence of the lattice disorder measured by RBS/C. However, an accurate determination of the structure or atomistic nature of the He$^+$ scattering centres in the form of disordered zones is difficult, precisely because RBS/C is far less sensitive than TEM for revealing such a damage at low fluence irradiation. The processes by which damage accumulates toward the eventual formation of an amorphous layer

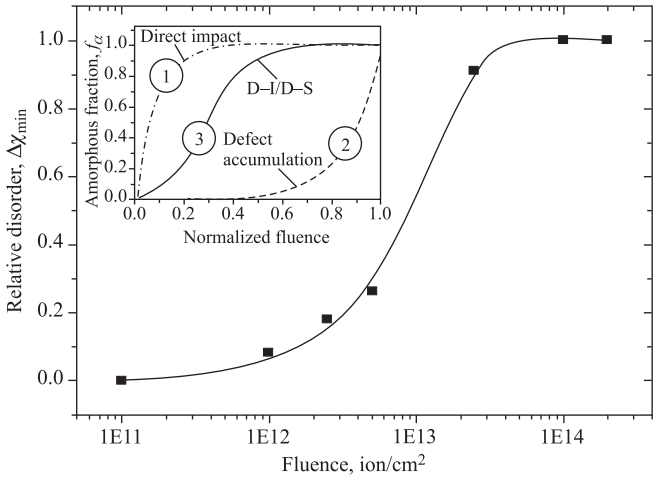

Fig. 3. A plot of relative disorder $\Delta\chi_{\min}$ vs ion fluence for 100 keV Au$^+$ ion irradiated InP. The best fit is obtained by using the modified Hecking model. The uncertainty for each ordinate data point is $\leqslant 5\%$. Inset graph is an idealized plot of the general three routes leading towards heavy-ion-induced amorphization in materials; the direct impact (heterogeneous; # 1), stimulated defect accumulation (homogenous; # 2) and both a combination of direct impact and stimulated defect accumulation (# 3)

in semiconductors have been generally described by defect overlap models based on statistics describing the ratio of the surface area covered by ion irradiation damage to the total area being irradiated [28]. These damage build-up models usually lie between the limiting extremes of two basic mechanisms defining two categories of amorphization process [28] as shown in the inset in Fig. 3. In the first, homogeneous nucleation (defect accumulation), amorphization occurs by the interaction and accumulation of simple point defects produced by irradiation until the defect density in a region of the irradiated lattice is so great that the region becomes unstable and spontaneously collapses to an amorphous state. In the second, heterogeneous nucleation (direct impact amorphization), small regions are directly amorphized during individual collision cascades and complete amorphization occurs by the accumulation and overlap of these regions. A detailed discussion and survey of various models can be found in Ref. [29].

Generally, amorphization in semiconductors can best be described by a combination of both heterogeneous and homogenous mechanisms. Composite models have been developed wherein an impinging ion can produce both a combination and coexistence of both point defects and amorphous zones which, when overlapping, convert to the amorphous state [29]. The relative amount of damage as a function of fluence in 100 keV Au^+ ion irradiated InP can be extracted from the RBS/C yield (Y); this is expressed as the relative disorder $\Delta\chi_{\min}$ defined as

$$\Delta\chi_{\min} = \frac{Y_{\text{irradiated}} - Y_{\text{unirradiated}}}{Y_{\text{random}} - Y_{\text{unirradiated}}}. \tag{1}$$

In this case, the value of $\Delta\chi_{\min}$ expresses the relative amount of disorder in the crystal and approaches unity for complete amorphization of at a fluence $\sim 2.5 \cdot 10^{13}$ ions/cm^2. The $\Delta\chi_{\min}$ calculated over the energy range of 1750–1850 keV (from Fig. 2) is plotted as a function of ion fluence in Fig. 3.

Here we invoked Weber's expansion of the Hecking model for the accumulation of damage [29, 30] as a realistic description of the amorphization process. In this model for description of damage accumulation an analytical expression is derived for the progression of amorphization which takes into account both types of damage. Thus, on the one hand, amorphization occurs heterogeneously (direct impact, i.e., each ion creates an amorphous zone) with probability P_a, and cross section for amorphization σ_a and f_a is the fraction of amorphous material. And on the other hand, taking into account homogeneous damage growth which is described by the overlap of pre-existing disorder (stimulated disorder, i.e., ions create an ensemble of point defects) with a stimulated defect production probability P_s and cross section for stimulated amorphization σ_s. The probability $P_i(f_a)$ for the amorphization process to occur is taken to be $f_a(1 - f_a)$. This direct-impact/defect-stimulated model is generally expressed as

$$df_a/dF = P_a(1 - f_a) + P_s f_a(1 - f_a). \tag{2}$$

The solution of the above equation [30] is expressed as follows:

$$f_a = 1 - (\sigma_a + \sigma_s)/(\sigma_s + \sigma_a \exp\left[\sigma_a + \sigma_s\right]\ F), \tag{3}$$

where F is the irradiating ion fluence.

From RBS/C spectra in Fig. 2, the best fit parameters for the plot of $\Delta\chi_{\min}$ vs ion fluence (i.e., Eq. (3) as shown in Fig. 3) are $\sigma_a = (5.99 \pm 0.64) \cdot 10^{-14}$ cm^2 and $\sigma_s = (5.91 \pm 2.13) \cdot 10^{-14}$ cm^2, with almost equal weights for both cross sections, suggesting a real role for *both* processes for damage build-up. The importance of both processes was also confirmed by recent MD simulations of primary damage for several elemental and compound semiconductors [31], the radiation damage due to a single ion can comprise either amorphous or disordered zones with point defects intimately involved, i.e., both heterogeneous and homogenous nucleation processes actually coexist. Amorphization, however, is not necessarily a simple phenomenon. Even if direct amorphization was to take place solely by means of heterogeneous nucleation [28] about the point at which each ion is ballistically stopped, factors such as point defects migration and recombination, local stoichiometric imbalance, dynamic annealing, the presence of impurities, sink effects such as surfaces, and the structure and variation of individual cascade damage can all play an important role. Furthermore, defects smaller than those resolved by TEM, point defects, for example, can play a significant role in the amorphization process [31]. From the TEM analysis of zones at the lowest irradiation fluence ($1 \cdot 10^{12}$ ions/cm^2), we have determined the size distribution of these zones as shown in Fig. 4. The data shown in Fig. 4 were obtained using the analySiS software package [27] determined by assuming that the area of each disordered zone is equivalent to the area of a circle, therefore calculating the

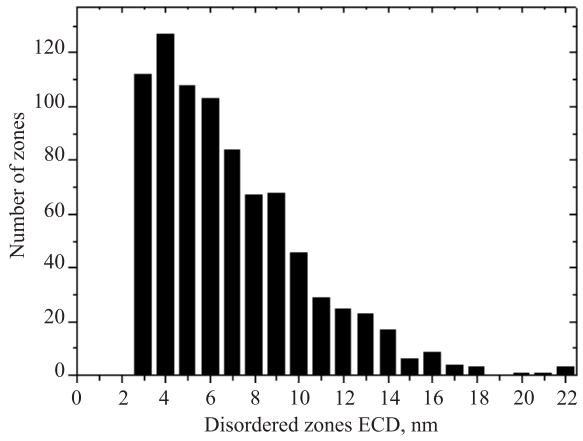

Fig. 4. Measured sizes of disordered zones in 100 keV Au^+ ion irradiated InP at a fluence of $1 \cdot 10^{12}$ ions/cm^2

diameter of the corresponding circle expressed as an Equivalent Circle Diameter (ECD) in nm, where $\mathrm{ECD} = 2\sqrt{A/\pi}$, where A is the area of a zone. These results were determined from a micrograph over a total area of 600×600 nm. Disordered zones ~ 2 nm in diameter or less could not be unambiguously resolved due to the finite resolution of TEM. Also, smaller radii would be physically meaningless, even if we were to assume that they are completely amorphous, given a minimum size requirement over which to define an amorphous phase within a crystalline lattice [32]. In addition, a difficulty is presented by defining the amorphous phase in InP, where the complex nature of the amorphous phase can encompass a multitude of configurations which have been either theoretically predicted or experimentally verified, which include coordination numbers ranging from three to six atoms and homopolar bonding of both In and P atoms [33]. However, we found that the density of these zones is less than the ion fluence. Thus, the density of TEM observed zones ~ 0.2 of the corresponding ion fluence ($1{\cdot}10^{12}$ ions/cm^2). An analogous yield (the areal density of zones per ion fluence) of less than unity ($\sim 0.4 - 0.5$) for InP *in-situ* irradiated by 50 keV Si^+ ions was also reported for irradiations at both room temperature and at 15 K [34]. This reported discrepancy between ion fluence and zone density does not suggest that this is due to an annealing process as it was carried out at very low temperature, but rather points to a strong probability for the existence of clusters which are not resolved by TEM. Similar observations for reduced defect yield were reported for 50 keV Kr^+, Xe^+ and Au^+ ion irradiation at 30 K in GaAs and GaP [35]. This also may further point to the necessity of a coexistence of homogenous nucleation mechanism and the subsequent overlap of disordered zones for complete amorphization, and that large proportion of damage might not be observed by TEM and that the observed zones are not necessarily amorphous in nature. Also, it should be emphasized that the energy loss process of an ion in the lattice is a statistical process and corresponds to the average over a series of single-energy-loss events. Therefore, it may be that not all the created damage can be resolved by TEM observation as each impinging 100 keV Au^+ ion can create simple point defects and/or defect clusters which are certainly not resolved by TEM or it can create damage in the form of disordered zones $\leqslant 1$ nm in size, but which can not be discerned by TEM observation. In addition, the action of surfaces as sinks for formed cascade defects must not be excluded. Furthermore, given the possibility of some overlap of zones at this ion fluence of $1 \cdot 10^{12}$ ions/cm^2, thus fluctuations in size and distribution of sizes of disordered zones are then unsurprisingly expected. Indeed, some observed zones are large and can reach 20 nm in diameter or more. However, the concentration of zones with small diameters (i.e., in the range $\sim 3 - 8$ nm) is the largest and the distribution is weighted towards smaller sizes, consistent with a theoretical study of size distribution of individual disordered and amorphous zones formation in semiconductors [36]. It must also be emphasized that zones *should* have a size distribution which can be wide and that variation

in size is expected. This is more realistic than assigning only one value for heavy-ion damage for the specified irradiation conditions as most models infer from the RBS/C measurements and the consequent modelling of the damage accumulation. We note here an observation made for medium-mass ion (300 keV Si^+ and 600 keV Se^+) irradiated InP [37]. However, in this work the authors used the simplest overlap Gibbons model [28] and inferred that overlap of zones is necessary for the creation of maximum damage in the form of completely amorphous layer [38].

In Fig. 5 we show an example of evolution of a field of such disordered zones under continuous 200 keV electron irradiation. As is evident in the above TEM images, continuous electron irradiation induces shrinkage and disappearance of disordered zones. For all the investigated electron energies (100–300 keV) the fraction of disorder was found to shrink gradually as a function of increasing electron fluences, where many zones completely disappeared. Quantification of the recovery process of disorder at all electron energies is presented in Fig. 6. In this graph, the total area of all the disorder as the sum of the areas of the observed dark contrast features (zones) normalized to the same initial pre-electron irradiated area (i.e., 0 electron fluence or 0 time) is plotted as a function of the electron fluence. The estimated errors in areal fraction determination (ordinate points) are approximately 5% for each ordinate point as this depends on the optimum threshold level for a micrograph sequence.

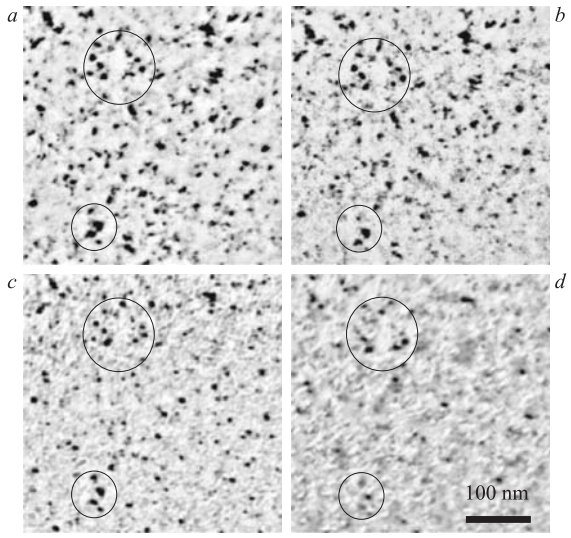

Fig. 5. TEM sequence of *in-situ* observations of disorderd zones recovery under 200 keV electron irradiation: before electron irradiation (*a*) and after electron fluence $\sim 6 \cdot 10^{21}$ e^-/cm^2 (*b*), $\sim 1.2 \cdot 10^{22}$ e^-/cm^2 (*c*) and $\sim 2.2 \cdot 10^{22}$ e^-/cm^2 (*d*). A couple of clusters of zones are circumscribed with circles

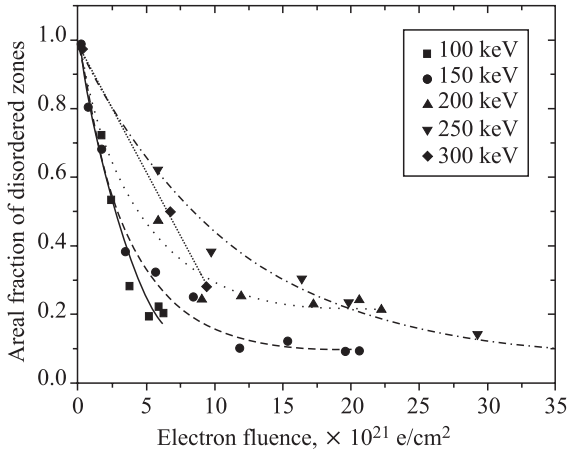

Fig. 6. Areal fraction of disordered zones as a function of electron beam irradiation fluence at different electron beam energies. The uncertainty for each ordinate data point is $\leqslant 5\%$

As apparent from Fig. 6, there is a continual recovery for all the energies investigated. This is evident as the continuous reduction of the areal fraction of disorder, where approximately half of the areal fraction of disorder recovers following irradiation to electron fluences of $\sim 0.5 - 1 \cdot 10^{22}$ e^-/cm^2. However, an enhanced recovery rate appears for the two lowest energies (100–150 keV), while the recovery is slower for the case of higher energies (200–300 keV).

Electron-beam-induced recovery is, in general, a complex process which has been attributed to a wide range of effects [39], mainly the following:

(1) Direct beam heating.

(2) Elastic interactions and knock-ons giving rise to enhanced point defects mobility.

(3) Electronic excitation involving the breaking or rearrangement of unstable bonds.

In order to asses and relate the temperature rise in InP to the energy loss of *in-situ* TEM irradiating electrons, we used the model of Fisher [40] based on the model of Gale and Hale [41], where it was assumed that a circular conductor of infinite conductivity held at fixed temperature T is bounding the specimen in the horizontal plane and that the irradiation was centered and had a Gaussian spatial distribution. Neglecting irradiative heat losses, the maximum temperature rise in the sample is given by

$$\Delta T = \frac{i}{4\,\pi\,k\,e}\left(\frac{dE}{dx}\right)\left(1 + 2\ln\frac{b}{r}\right), \tag{4}$$

where ΔT is the rise in temperature, i is the current of the electron beam, k is the thermal conductivity of the medium, i.e., for InP = 0.68 W cm^{-1} $^\circ C^{-1}$ [42],

where $\left(\frac{dE}{dx}\right)$ is the inelastic energy loss of electrons (stopping power) in InP expressed in eV/nm. The mean energy loss by electronic excitation (i.e., inelastic) expressed in MeV/cm for irradiating electrons in the relativistic region is given by the well-known Bethe–Bloch expression [43]:

$$-\frac{dE}{dx} = \frac{5.09 \cdot 10^{-25} n}{\beta^2} \times \left[\ln \frac{3.61 \cdot 10^5 \tau \sqrt{\tau + 2}}{I_{ev}} + F(\beta)\right] \text{ MeV/cm}, \quad (5)$$

where

$$F(\beta) = \frac{1 - \beta^2}{2} + \frac{1}{2(\tau + 1)^2}\left[\frac{\tau^2}{8} - (2\tau + 1)\ln 2\right] \quad (6)$$

and $\beta = V/c$ is the speed of the electron relative to the speed of light in vacuum, n is the number of electrons per unit volume in the medium, $\tau = T/mc^2$ is the kinetic energy T of the electron expressed in multiples of the electron rest energy mc^2, and I_{ev} is the mean ionization energy of the target atoms. The parameter b in Eq. (4) is the diameter of the standard TEM sample (3000 μm) and r is the electron beam radius (~ 1 μm). Clearly, Eq. (4) demonstrates that the temperature rise is proportional to the beam current $i_{\max}$ (~ 8.3 nA), inversely proportional to the thermal conductivity k and the beam radius r and is independent of the foil thickness. Figure 7 shows a plot of inelastic energy loss of electrons vs the electron energy in InP calculated for a wide range of electron energies. As evident in that figure, for 100 keV electrons in InP, the inelastic energy loss $\left(\frac{dE}{dx}\right) \approx 4$ eV/nm and, assuming that it is constant through the thin foil sample, the temperature rise in an area illuminated by an electron beam having a radius $r = 1$ μm would be $\sim 3\,^{\circ}$C. At higher electron energies, the temperature rise is

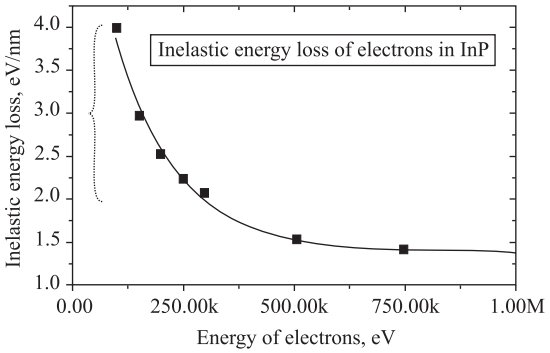

Fig. 7. Electron inelastic energy loss (eV/nm) as a function of electron energy. The dotted bracket encompasses the inelastic energy loss range for the utilized electron beam energies (100–300 keV)

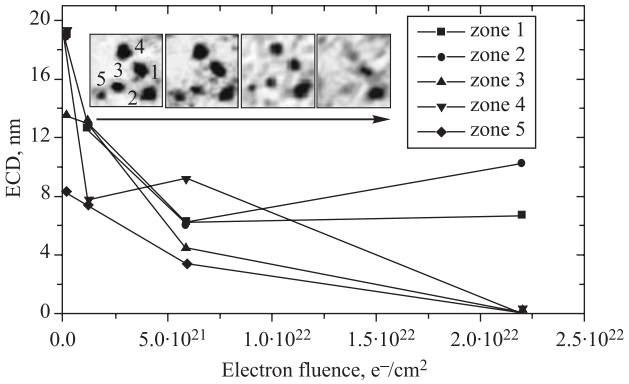

Fig. 8. Equivalent circle diameter (ECD) in nm of five zones annealed by 200 keV electron irradiation. Three zones disappear (zones: 3, 4 and 5), while two zones remain (zones: 1 and 2) after shrinkage at a high fluence of electrons $\sim 2.2 \cdot 10^{22}$ e^-/cm^2

expected to be even less given the reduction in energy loss apparent in Fig. 8. Therefore, in performing the *in-situ* electron irradiation experiments with a well-spread beam and small electron current, direct beam heating of the InP sample can be safely neglected, and we need to only concern ourselves with the primary radiation processes induced by the electron beam [39].

Thus, given the very slight increase in the temperature of the sample under the utilized *in-situ* electron beam conditions, the direct heating effects can be excluded. This was further supported by the TEM observation of areas at approximately one electron beam diameter away (~ 2 μm) from the *in-situ* electron irradiated areas after the end of each electron irradiation experiment. The disordered zones were found to be intact in these areas with almost no change or decrease in contrast or areal fraction, eliminating the possibility of heat generation and thermal conduction. Furthermore, from previous similar electron beam irradiation experiments on Si and Ge, *in-situ* electron-beam-induced recovery was found to be insensitive to the temperature (30 and 295 K) at which the sample was maintained [3]. Thus, these observations also support that electron-induced recovery in InP is already not a thermal effect which roles out the first case. For the second case, which involves elastic interaction collisions from the electron beam, this arises when the electron energy is sufficient elastically to displace atoms in the irradiated material ($\geqslant E_d$). Thus, recovery could be simulated by ballistic transfer of kinetic energy from an electron to a lattice atom. However, for binary semiconductor compounds, there are different values of maximum energy transfer between the constituent atoms. In the case of InP this is more pronounced because of the much lighter mass of P compared to In (mass ratio of 3.7), which yields threshold electron energies for displacing P and In atoms of ~ 110 and

270 keV, respectively, assuming that the mean displacement energies (E_d) of In and P are 6.6 and 8.8 eV, respectively [44]. The maximum energy transferred in an elastic collision between an electron and either P or In atom in InP, can be obtained using equation of maximum energy transfer from an impinging electron $T_{\max}(\mathrm{eV})$ as follows [45]:

$$T_{\max} = \frac{4M_1M_2}{(M_1+M_2)^2}E, \tag{7}$$

where M_1 and M_2 are the masses of the electron and the target atom, respectively, and E is the energy of the impinging electron (100–300 keV). One then is able to calculate the maximum energy elastically transferred ($T_{\max}$) to In and P atoms by the irradiating electrons in InP for the 100–300 keV electron beam energies, as indicated in Table.

The maximum elastic energy transfer $T_{\max}$ (eV) to In and P atoms due to electron-atom-knock-on elastic collisions

Electron energy (keV)	100		150		200		250		300	
Atoms	In	P	In	P	In	P	In	P	In	P
$T_{\max}(\mathrm{eV})$	2.1	7.8	3.3	12.3	4.6	17	6	22.2	7.4	27.6

For the case of elastic energy transfer by impinging electrons, in addition to the point defects introduced by simple electron-atom-knock-on, the heavy-ion irradiation of compound semiconductors such as InP may introduce a greater variety of point defects and point defects complexes than in elemental semiconductors, for example. These defects can also further participate in the electron-beam-enhanced recovery. For electron energies above the displacement threshold for both In and P atoms, we expect Frenkel defects on both In and P sublattices. It is likely that the disordered zone recovery that does occur is associated with electron-beam-stimulated recombination of mobile point defects, i.e., In and P interstitials with their corresponding vacancies introduced by electron irradiation and possibly with the participation of small defect clusters which were already created due to the heavy-ion irradiation itself. Also, the elastic mechanism can potentially operate at energies slightly below the displacement threshold for both constituent atoms, since a slightly lower energy may be needed to displace an atom inside or at the disordered zone interface than one in an intact lattice site because the number of defect states available to the system is larger than that in intact lattice sites [46]. It should also be noted that recovery of disorder may also depend on the availability of the elements in the correct proportion at the interface between the damaged and undamaged material. A stoichiometric imbalance produced during heavy-ion irradiation [47, 48] may stimulate diffusion in order to restore the *status quo* [49].

Our observations of an enhancement of disorder recovery at 100 and 150 keV as shown in Fig. 8, where electrons at 100 keV energy are definitely not capable of displacing either P or In atoms in InP, imply the role of inelastic energy transfer in recovery process of disordered zones. Nevertheless, the inelastic electron energy loss at this energy is higher by a factor of ~ 2 than that at 300 keV as indicated in Fig. 6.

This leads us to the third effect, where the inelastic energy, in the form of electronic excitation (ionization) processes, could be transferred to the lattice and plays a dominant role in the annealing and shrinkage of disorder at 100 keV or subthreshold electron energies (electrons with energies not capable of direct displacement of either In or P atoms) in general. This assertion is very plausible because electronic excitation can indeed induce atomic motion and rearrangement [50] and indeed, the whole field of ion track physics, for example, is build on that assertion. Recovery at 100 keV electron beam energy has also been observed in 50 keV Si^+ irradiated InP [14]. Furthermore, as mentioned in the introduction, increased recovery rate under subthreshold electron beam irradiation has been observed in isolated disordered or amorphous zones for both elemental and compound semiconductors irradiated with heavy ions (50–300 keV Xe^+), where the efficiency of the electron-induced recovery process further increases at electron energies below 100 keV [1]. Not only isolated disordered zones, but also continuous amorphous layers can recover, and crystallinity is restored under 100 keV electron beam irradiation as observed for the case of other compound semiconductor GaAs [51].

However, the exact inelastic transfer mechanism responsible for the observed recovery by 100 keV electrons is not yet clear or well understood. The transferred inelastic energy by subthreshold electrons might induce local modification in the heavy-ion disordered lattice manifested by bond scission and rearrangements, especially for covalent bonds in the periphery of a zone [50], this may effectively lower the barrier for defect and disorder recovery of the lattice. Indeed, recent MD simulation by Frantz et al. [22] has shown that in the case of amorphous zones embedded in a covalently bonded crystalline lattice, there is a continuous recovery process under subthreshold electron energies irradiation even at very low temperatures (approaching 0 K) of the lattice containing these zones. In this reported work, the individual bonds between atoms were randomly switched off for a short period of time. The results of this process depend on the chosen parameters of this bond breakage model, but in all cases the zone shrinkage rate was proportional to the total number of *bond switches* initiated by irradiating electrons. This can be further assisted by the presence of defects at the disordered/amorphous zones and their irregular shaped interfaces, which offer a large number of preferential regrowth sites and which may further lower the required electron energies for recovery processes [2, 52]. It was concluded that the zone recovery process may be due to an athermal bond breakage and rearrangement

process at the amorphous/crystalline (a/c) interface induced by an inelastic energy transfer mechanism [22]. Similar to our own observations, we note here that an enhanced electron-beam-induced recovery of zones was observed at even lower electron energies (< 50 keV) than in our own work for other compound semiconductors such as GaAs and GaP [35].

These further emphasize the role of the inelastic energy loss processes and their effects in the case of electron beam irradiation of semiconductors, similar to the well-established observations of ion-beam-induced epitaxial recrystallization reported, for example, in the case of amorphous GaAs [53].

An important fact which should be emphasized here is that the recovery of a nanometer-sized disordered volume as the zones we observe in InP involves several hundred atomic rearrangements. In addition, MD simulations have shown that local fluctuations in atomic densities between disordered zones are to be expected [31, 54]. Thus, the irregularity of the interface of any zone and the variation in local atomic density, arrangement and stoichiometric imbalance inside or at the interface of a zone give each zone a *unique individuality*, which is quite different from the case for planar amorphous layers, for example, where a regular interface exists between the amorphous or disordered lattice and the intact lattice. Also, the contrast of a zone as observed in TEM depends on its longitudinal dimension along the sample thickness. And it should be remembered that TEM observation is only a two-dimensional representation of a three-dimensional phenomenon which may introduce further complication for zones recovery relative to that of planar amorphous interface, for example. This is evidenced in Fig. 8, which shows the recovery in the form of shrinkage and disappearance of five individual zones under the same illuminating electron fluences for 200 keV electron beam energy. The recovery proceeds rapidly initially; three zones disappear completely whilst two zones remain after reaching an electron fluence

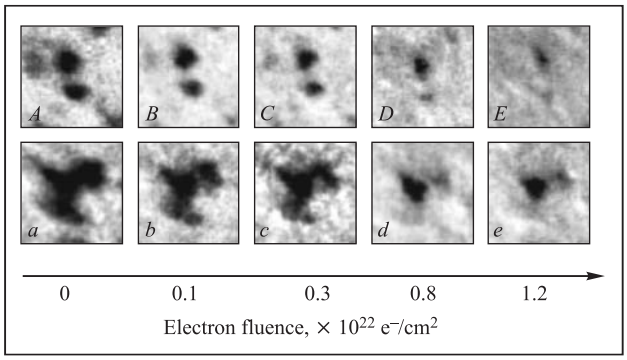

Fig. 9. A sequence of TEM micrographs illustrating the 150 keV electron-beam-induced recovery of individual disordered zones (the side of each micrograph is 40 nm). Smaller zones appear to anneal faster than the larger ones

of $\geqslant 2 \cdot 10^{22}$ e^-/cm^2. In a similar way, Fig. 9 illustrates the recovery of individual zones due to 150 keV electrons under the same irradiation fluences. In this case, two zones almost similar in size are depicted in the upper sequence $(A - E)$; one zone recovers before the other whilst in the lower sequence $(a - e)$ the recovery of a large disordered zone, which might consist of three individual smaller zones, is slower. This clearly shows that zone sizes have no relevance in the kinetics of their electron-beam-induced recovery. Quite similarly to our observations, in TEM *in-situ* investigation for thermal-induced recovery of amorphous zones in silicon, Donnelly et al. [55] found that the total areal fraction of all zones continued to decrease (anneal) upon heating of the sample. However, despite this overall decrease, individual zones exhibit an erratic recovery behaviour. No consistency in their behaviour with no well-defined correlation between their size and recrystallization temperature was observed as zones with similar size crystallized over a wide temperature range encompassing $\sim 300\,^{\circ}C$. In another recent TEM observation on 200 keV Xe^+ ion irradiated Si, Donnelly et al. [56] showed that size alone is not unique determinant of the temperature at which a zone will anneal (completely recover). Zones of similar starting size do not recover at the same temperature. In some cases even several zones start to grow rather than shrinking, this was termed a «*reverse annealing*» step which is very plausible as a zone of proximity of another zone may grow on the expanse of the nearby shrinking zone by «absorbing» the annihilated defects from the later zone.

Thus, the recovery process of individual zones, either thermally or electron-beam-induced as in our case, might not be a singly activated process at all and each individual zone may have a different «triggering» energy for the onset of recrystallization. This also suggests that the recovery kinetics primarily depends on the disordered zone-crystal interface. And consideration of local topology and the local radius of curvature of a disordered/amorphous zone-crystal interface may play a crucial role and be responsible for different activation energies. As recently shown by MD simulations for disorder in Si, the recovery of a given amount of disorder strongly depends on its spatial distribution [57]. Indeed, as suggested by Carter [58] in a theoretical investigation on the annealing of zones, there may well exist a wide population of activation energies for which the mean activation energy increases with the amorphous or disorder fraction in the material. Therefore, we can generally infer that the recovery of individual zones in a volume is a much more complicated process than previously studied processes of planar a/c interface annealing under electron beam irradiation might suggest [59–61].

CONCLUSIONS

The damage created in InP single crystals by 100 keV Au^+ ions in the form of disordered zones for low-fluence ion irradiation was observed by TEM. These

zones are characterized by an irregular shape and distribution in sizes and their density is lower than the ion fluence. The exact atomistic nature of damage inside these zones can not be determined unambiguously either by TEM or RBS/C. The damage increases with ion fluence until complete amorphization is reached at ion fluences $\geqslant 2.5 \cdot 10^{13}$ ions/cm^2. The best fit for the relative disorder induced by 100 keV Au^+ ion irradiation of InP from the RBS/C yields was obtained using the modified Hecking model which takes into account both heterogeneous (direct impact) and homogenous (defect stimulated) amorphization. Thus, damage accumulation is best described by the invocation of both coexisting heterogeneous and homogenous nucleation processes in low-energy heavy-ion irradiated InP. Electron-beam-induced recovery of zones was observed *in-situ* in InP as a function of electron energies and fluences. Zones were found to be sensitive to irradiating electrons, where they shrink and disappear even at *subthreshold* electron energies (insufficient to displace either P or In atoms in InP). An important role for inelastic mechanisms in the recovery process is strongly implied. And it appears to be unnecessary to suppose that only elastically produced Frenkel pairs induce recovery. It is more likely that electron-beam-induced ionization (electronic excitation) may play a significant role in the solid-phase recovery process of disorder in InP. The shrinkage and disappearance of zones by electron beam irradiation do not depend on the zone size and which might not be singly activated process as the case for recovery of planar amorphous interface.

REFERENCES

1. *Jencic I., Hollar E. P., Robertson I. M.* // Philosophical Magazine. 2003. V. 83. P. 2557–2571.
2. *de la Rubia T. D.* // Annual Review of Materials Science. 1996. V. 26. P. 613–649.
3. *Jencic I. et al.* // J. of Appl. Phys. 1995. V. 78, No. 2. P. 974–982.
4. *Jencic I., Robertson I. M.* // J. of Materials Research. 1996. V. 11, No. 9. P. 2152–2157.
5. *Parsons J. R., Balluffi R. W., Koehler J. S.* // Appl. Phys. Lett. 1962. V. 1. P. 57.
6. *Howe L. M., Rainville M. H.* // Nucl. Instr. Meth. B. 1987. V. 19/20. P. 61.
7. *Narayan J. et al.* // Materials Letters. 1984. V. 2, No. 3. P. 211–218.
8. *Howe L. M., Rainville M. H.* // Nucl. Instr. Meth. 1981. V. 182/183. P. 143.
9. *Ruault M. O. et al.* // Philosophical Magazine. A. 1984. V. 50, No. 5. P. 667–675.
10. *Bernas H., Ruault M. O., Zheng P.* Multiple Amorphous States in Ion Implanted Semiconductors Si and InP. Crucial Issues in Semiconductor Materials and Processing Technologies / Ed. S. Coffa. Netherlands: Kluwer Academic Publishers, 1992.
11. *Chadderton L.* // Radiation Effects. 1971. V. 8. P. 77–86.
12. *Chandler T. J., Jenkins M. L.* The Structure of Displacement Cascades in III–V Semiconductors. Series 67, 1983. Microscopy of Semiconductor Materials. Institute of Physics Conference, London.

13. *Jenkins M. L. et al.* In-situ Observations of the Development of Heavy-Ion Damage in Semiconductors. Series 79, 1985. Microscopy of Semiconductor Materials. Institute of Physics Conference, London.
14. *Zheng P. et al.* // J. of Phys. D. 1990. V. 23. P. 877–883.
15. *Ruault M. O., Chaumont J., Bernas H.* // Nucl. Instr. Meth. 1983. V. 209/210. P. 351–356.
16. *Jencic I., Hollar E. P., Robertson I. M.* // Nucl. Instr. Meth. B. 2001. V. 175. P. 197–201.
17. *Robertson I. M., Jencic I.* // J. of Nuclear Materials. 1996. V. 239, No. 1–3. P. 273–278.
18. *Bench M. W. et al.* // J. of Appl. Phys. 2000. V. 87, No. 1. P. 49–56.
19. *Jencic I. et al.* // Nucl. Instr. Meth. B. 2002. V. 186. P. 126–131.
20. *Jencic I., Robertson I. M.* Regrowth of Heavy-Ion Implantation Damage by Electron Beams // Materials Science in Semiconductor Processing. 2000. V. 3, No. 4. P. 311–315.
21. *Jencic I., Robertson I. M., Skvarc J.* // Nucl. Instr. Meth. in Phys. B. 1999. V. 148, No. 1–4. P. 345–349.
22. *Frantz J. et al.* // Phys. Rev. B. 2001. V. 64, No. 12. Art. No. 125313.
23. AnalySIS®, Soft Imagining System, http://www.soft-imaging.net
24. *Russ J. C.* Computer-Assisted Microscopy: the Measurement and Analysis of Images. N. Y.: Plenum, 1990.
25. *Jenkins M. L., Kirk M. A.* Characterization of Radiation Damage by Transmission Electron Microscopy. Series in Microscopy in Materials Science, 2001, London, Institute of Physics.
26. *Bench M. W., Tappin D. K., Robertson I. M.* // Philosophical Magazine Letters. 1992. V. 66, No. 1. P. 39–45.
27. The Stopping and Range of Ions in Matter, http://www.srim.org
28. *Gibbons J. F.* Ion Implantation in Semiconductors. II. Damage Production and Annealing // Proc. of the Institute of Electrical and Electronics Engineers. 1972. V. 60, No. 9. P. 1062–1096.
29. *Weber W. J.* // Nucl. Instr. Meth. B. 2000. V. 166/167. P. 98–106.
30. *Hecking N., Heidemann K. F., Kaat E. T.* // Nucl. Instr. Meth. B. 1986. V. 15. P. 760–764.
31. *Nord J., Nordlund K., Keinonen J.* // Phys. Rev. B. 2002. V. 65. Art. No. 165329.
32. *Cohen C. et al.* // Phys. Rev. B. 1985. V. 31. P. 5–14.
33. *Bezakova E. et al.* // Appl. Phys. Lett. 1999. V. 75, No. 13. P. 1923–1925.
34. *Zheng P. et al.* // J. of Appl. Phys. 1991. V. 70, No. 2. P. 752–757.
35. *Bench M. W.* Transmission Electron Microscopy Investigation of Ion Implantation Damage in GaAs and Other Semiconductors. Ph. D. Thesis, 1992, University of Illinois at Urbana-Champaign.
36. *Kucheyev S. O.* // Nucl. Instr. Meth. B. 2001. V. 174, No. 1–2. P. 130–136.
37. *Wendler E. et al.* // Nucl. Instr. Meth. B. 1995. V. 106, No. 1–4. P. 303–307.

38. *Wendler E., Opfermann T., Gaiduk P. I.* // J. of Appl. Phys. 1997. V. 82, No. 12. P. 5965–5975.
39. *Hobbs L. W.* Radiation Damage with Biological Specimens and Organic Materials // Introduction to Analytical Electron Microscopy / Eds. John. J. Hern, I. Joseph I. Goldstein, and David C. Joy. N. Y.: Plenum Press, 1979.
40. *Fisher S. B.* // Radiation Effects. 1970. V. 5. P. 239.
41. *Gale B., Hale K. H.* // British J. of Appl. Phys. 1961. V. 12. P. 115.
42. http://www.ioffe.rssi.ru/SVA/NSM/Semicond/InP/thermal.html
43. *Barnett R. M. et al.* // Review of Particle Physics, Phys. Rev. D. 1996. V. 54, No. 1. P. 1–708.
44. *Vavilov V. S., Kiv A. E., Niyazova O. R.* // Phys. Status Solidi a. 1975. V. 32. P. 11–33.
45. *Chadderton L. T.* Radiation Damage in Crystals. London: Methuen, 1964.
46. *Caturla M. J., de la Rubia T. D., Gilmer G. H.* // J. of Appl. Phys. 1995. V. 77, No. 7. P. 3121–3125.
47. *Nordlund K., Nord J., Keinonen J.* // Nucl. Instr. Meth. B. 2001. V. 175. P. 31–35.
48. *Christel L. A., Gibbons J. F.* // J. of Appl. Phys. 1981. V. 52, No. 8. P. 5050–5055.
49. *Speriosu V. S. et al.* // Appl. Phys. Lett. 1982. V. 40, No. 7. P. 604–606.
50. *Itoh N., Stoneham M. A.* Materials Modification by Electronic Excitation. London: Cambridge University Press, 2001.
51. *Yang X. et al.* // Materials Science and Engineering B. 1997. V. 49. P. 5–13.
52. *Liu G-Q., Nygren E., Aziz M. J.* // J. of Appl. Phys. 1991. V. 70, No. 10. P. 5323–5345.
53. *Kobayashi N. et al.* // Nucl. Instr. Meth. B. 1991. V. 59/60. P. 449.
54. *Nord J., Nordlund K., Keinonen J.* // Nucl. Instr. Meth. B. 2002. V. 193, No. 1–4. P. 294–298.
55. *Donnelly S. E. et al.* // Appl. Phys. Lett. 2003. V. 82, No. 12. P. 1860–1862.
56. *Donnelly S. E. et al.* // Nucl. Instr. Meth. B. 2006. V. 242, No. 1–2. P. 595–597.
57. *Marques L. A. et al.* // Computational Materials Science. 2003. V. 27, No. 1–2. P. 6–9.
58. *Carter G.* // J. of Phys. D: Appl. Phys. 1996. V. 29. P. 1619–1623.
59. *Lulli G., Merli P. G.* // Phys. Rev. B. 1993. V. 47. P. 4023–4301.
60. *Lulli G., Merli P. G., Antisari V.* // Phys. Rev. B. 1987. V. 36. P. 8038–8042.
61. *Lulli G., Merli P. G., Antisari V.* Solid Phase Epitaxy if Implanted Silicon Induced by Electron Irradiation at Room Temperature // Materials Research Symposium Proceedings. 1988. V. 100. P. 375–380.

Received on May 26, 2008.

Редактор *В. В. Булатова*

Подписано в печать 04.08.2008.
Формат 60 × 90/16. Бумага офсетная. Печать офсетная.
Усл. печ. л. 1,5. Уч.-изд. л. 2,06. Тираж 280 экз. Заказ № 56285.

Издательский отдел Объединенного института ядерных исследований
141980, г. Дубна, Московская обл., ул. Жолио-Кюри, 6.
E-mail: publish@jinr.ru
www.jinr.ru/publish/